Separation and Purification Technology 279 (2021) 119704

Contents lists available at ScienceDirect

Separation and Purification Technology

journal homepage: www.elsevier.com/locate/seppur

Amide functionalized DWCNT nanocomposite membranes for chiral separation of the racemic DOPA

Monti Gogoi [a,b], Rajiv Goswami [a,b], Alimpia Borah [a,b], Hrishikesh Sarmah [a], Parashmoni Rajguru [a], Swapnali Hazarika [a,b,*]

[a] Chemical Engineering Group, Engineering Sciences & Technology Division, CSIR-North East Institute of Science and Technology, Jorhat, Assam 785006, India
[b] Academy of Scientific and Innovative Research (AcSIR), Ghaziabad 201002, India

ARTICLE INFO

Keywords:
Enantiomers
Surface modification
Chiral separation
DOPA
Nanocomposite membrane

ABSTRACT

In view of the demand for enantiopure compounds of drug molecules, a new strategy was developed to improve the enantioseparation performance of a racemic mixture of 3,4-dihydroxyphenylalanine (DOPA) with the help of a functionalized Double-walled Carbon Nanotube (DWCNT) membrane. With the aid of covalent oxidation followed by an amidation reaction, chiral selectors, namely L-tryptophan and L-DOPA were incorporated separately into the DWCNT solution phase. The corresponding hybrid dispersions were assembled into two nanocomposite membranes ($M_{L\text{-tryp}}$ and $M_{L\text{-DOPA}}$) via vacuum-assisted filtration. The enantioselective performance of each membrane was evaluated by conducting permeation experiments. The time-dependent membrane permeation results have shown an enantiomeric excess value of up to 99% for the $M_{L\text{-DOPA}}$ and 98% for the $M_{L\text{-tryp}}$ membrane. Due to the self-linkage across the amide layer grafted on the FDWCNT surface, the L-isomer from the racemic mixture of DOPA was preferentially adsorbed onto the membrane, which has also been established by considering three-point interaction model. In contrast, the D-isomer was permeated through the nanoporous membrane. This tradeoff in permeation results in a high flux value for D-isomer (37.44 $mmol \cdot m^{-2} \cdot h^{-1}$) with concomitant lowering of the flux value for L-isomer (0.35 $mmol \cdot m^{-2} \cdot h^{-1}$) at an applied pressure of 5 bar was observed. The peclet number for both the membranes was found to be ~500, which can be attributed to the higher convective velocity of the fluid through bulk transport phenomena in a continuous manner.

1. Introduction

Chirality is an intriguing term that plays a vital role in pharmaceutical, agricultural, and other chemical industries [1]. On a specific note, the urge to achieve an enantiomerically pure form of a racemic drug in the pharmaceutical industry is of tremendous concern, as among the two possible enantiomers, one has pharmacological, pharmacokinetic and pharmacodynamic effects on human health. In contrast, its antipode has adverse side effects [2–3]. In response to the thriving necessity of single-enantiomer drugs to imbue safety and potency, considerable research efforts have been put forward to design new strategies for bulk scale resolution of racemic mixtures. The conventional methods of chiral separation like enzyme-assisted resolution [4], solid residue crystallization [5,6] silica-based chromatographic process [3] have been employed for a long time for analytical enantiomeric separation. But they suffer from several decisive drawbacks, including massive energy consumption, high operational cost, low performance, and discontinuous operation process [7]. To circumvent this limitation, developing a novel separation technique is the vital requirement of the hour. Fortunately, the membrane-based chiral separation technique has provided an alternative platform to achieve an enantiomerically pure isomer, which is simple in operational techniques and convenient for cost-effectiveness. It has high separation performance, enabling a viable platform to achieve industrial-scale enantiomeric separation [7–8].

The enantioselective solid-state membranes that have been reported in earlier literature are either based on the diffusion-enantioselective process or the enantioselective adsorption process [9–10]. Out of the two candidates, the adsorption-enantioselective membranes are superior in terms of high flux and enantioselectivity [11]. Different polymeric membranes incorporating chiral selector moieties have been demonstrated to achieve chiral separation of pharmaceutically important compounds. But they are also inadequate when crucial parameters

* Corresponding author at: Chemical Engineering Group, Engineering Sciences & Technology Division, CSIR-North East Institute of Science and Technology, Jorhat, Assam 785006, India.
E-mail address: shrljt@yahoo.com (S. Hazarika).

https://doi.org/10.1016/j.seppur.2021.119704
Received 8 July 2021; Received in revised form 7 September 2021; Accepted 9 September 2021
Available online 13 September 2021

like membrane mechanical stability, fouling property, etc., are concerned [12,13].

Recently, the carbon-based material has been utilized as a new one rather than the conventional polymeric membrane in separation technologies due to its exceptional atomic thickness, lamellar 2D structure, high thermal and chemical stability, antifouling property, and high tensile strength [14]. The interlayer galleries of the 2D membrane can be tuned with the desired functional group before self-assembling, which helps in impregnating the chiral selector into its voids spaces and provides a special co-relation between their permeation and selectivity. In that context, Meng et al. reported a graphene oxide membrane (GO) functionalized with an L-Glu chiral selector and a large carboxyl-terminated ionic liquid (IL-COOH) as the molecular spacer to achieve high-throughput enantiomeric separation of DL-3,4-dihydroxyphenylalanine (the racemic mixture of DOPA) [15]. Wang et al. reported a graphite phase carbon nitride (GCN) membrane embedded with (1R) -(−)-10-camphor sulfonic anion (CSA) as the chiral selector as well as a molecular spacer to separate limonene racemates under concentration gradient driving force and achieved ee value up to 89% [16].

Although 2D carbon-based membranes like GO and GCN show excellent selectivity in separation performance for chiral separation, they usually suffer from lower permeability issues [17]. However, for industrial-scale separation, the potential source of the membrane-assisted process is examined by the preferred way of membrane permeability and adequate selectivity. In that context, the Carbon nanotube is a superior candidate of choice and the unprecedented permeability of the CNT membrane is well documented in the literature [18]. However, CNTs are hydrophobic, which limits their utilization in biochemical and biomedical applications. Fortunately, the functionalization of CNT paved a way to make it partially hydrophilic which renders its application in the field of chiral separation. For the first time, our group recently reported a functionalized single-walled carbon nanotubes (FSWCNT) thin-film membrane with D-tryptophan as a chiral probe to separate tyrosine racemates with external pressure gradient [14]. The present work demonstrates the utilization of a double-wall carbon nanotube (DWCNT) membrane to separate racemates of the racemic mixture of DOPA. In our case, the functional surface controls much of the chiral separation performance. In addition to that, the membrane matrix also plays a significant role in the overall separation performance when durability and fouling resistance is concerned. A preferred membrane matrix in molecular separation is that which is thermally, chemically and mechanically robust. As a synthetic blend of both SWCNTs and MWCNTs, DWCNT possess superior thermal, chemical and mechanical stability, along with excellent flexibility. Moreover, any structural defect in SWCNTs induced during surface modifications can alter their mechanical and chemical properties in functionalized form. Hence, they may become more vulnerable to fragmentation via C═C bond breakages. On the other hand, only the outer wall of DWCNT is modified, keeping its internal layer and inherent properties intact. On a specific note, CNT is preferred over graphene/graphene oxide. In the re-assembled graphene-based membrane, the preferred water transport pathway is zig-zag, which involves horizontal and vertical water transportation across the percolated nano-capillaries between adjacent graphene sheets. On the other hand, the preferred orientation of CNT in the membrane matrix is relatively vertical, which eventually mitigated the lower permeability issues related to horizontal transportation mode [19–24].

Taking advantage of the superiority of DWCNT, we have demonstrated a functionalized Double-walled Carbon nanotube (DWCNT) membrane for enantioseparation of a racemic mixture of DOPA. The functionalization of the outermost stacked layer of DWCNT was carried out by grafting the reactive amide linkage, enhancing the chemical activation of graphitic carbon. The amide linkage was developed through the consecutive introduction of L-tryptophan and L-DOPA to different stock solutions. The pressure-driven membrane permeation experiment was carried out using two-compartment membrane cells to study the permeation experiment. The enantioselective adsorption behavior of $M_{L\text{-}DOPA}$ and $M_{L\text{-}tryp}$ exhibited the stronger binding affinity of L-isomer of the racemic mixture of DOPA into the L-DOPA and L-tryptophan, respectively.

2. Experiment

2.1. Materials

The raw standard Double-walled carbon Nanotubes, DWCNT (OD: 2–4 nm, assay: min. 60%, Length: 0.5–2 μm) and Polyethylene Glycol (PEG) were purchased from M/s Sisco Research Laboratory Pvt. Ltd (SRL), Mumbai, India. M/s SIGMA-Aldrich provided the polymeric material Polysulfone having a molecular weight of 30,000. The chlorinating agent Thionyl Chloride was purchased from M/s Merck Specialities Private Limited, Mumbai, India. M/s RANKEM range of laboratory chemicals, Gujarat, India supplied Ethanol (C_2H_5OH), hydrogen peroxide (H_2O_2), Dimethylformamide ($HCON(CH_3)_2$), Sulphuric acid (H_2SO_4), and Methanol (CH_3OH) to initiate the functionalization of DWCNT. The solvent N-methyl pyrrolidine (NMP), our samples of interest DL-, D- and L-3,4-dihydroxyphenylalanine and L-tryptophan were provided by the supplementary source of M/s TCI Chemicals.

2.2. Functionalization of DWCNT

The functionalization of DWCNT is one of the most integral pathways to carry out their reactive affinity towards organic drugs. The segregation of CNT clusters was carried out with the help of ultrasonic treatment. Typically, 15 mg of pure DWCNT under an ethanolic environment was sonicated for about 45 min, followed by vacuum filtration of the sonicated solution equipped with a Poly Tetra Fluoro Ethylene (PTFE) membrane to get residual mass. Then the solid residual mass of DWCNT was oven-dried at 100 °C to ensure complete dehydration.

To introduce acidic moieties into the as-prepared segregated DWCNT, 5 mg of DWCNT was agglomerated in 6.5 mL peroxide assisted acidic solution mixture at a ratio of 1:3 (v/v) through ultrasonic treatment at 30 °C for about 6 h. The unreactive DWCNT part and the excess acid were removed via filtering through a PTFE membrane (pore size of 0.2 μm) followed by continuously passing water until a neutral pH is achieved. The as-obtained acid functionalized DWCNT was then oven-dried at 120 °C.

Transformation of acid functionalized DWCNT into its corresponding acid-chloride (—COCl) was mediated by treating 5 gm of acid-activated DWCNT with a definite ratio (12:1 (v/v)) of Thionyl chloride in Dimethylformamide (DMF) under controlled reflux condition for a duration of 52 h. The temperature of the solution mixture was brought down to room temperature, followed by vigorous rinsing with 10 mL of unimolar ratio of ethanolic THF solution of ratio 1:1 (v/v). Then, the mixture was filtered out and dried overnight.

Finally, amidation of the DWCNT phase bearing the acid-chloride moieties was performed, enabling incorporating the chiral selectors in the parent DWCNT surface. Further, the reaction was performed by taking 5 gm of -COCl functionalized DWCNT in a solution containing a 3:1 (v/v) water/ethanol mixture. Then 15 g of each L-tryptophan and L-DOPA were added to the above mixture in two different round bottom flasks and agitated under reflux conditions for about 8 h. Resultant solid mass was segregated separately by filtration method and oven-dried. The excess unreacted residue of L-tryptophan and L-DOPA were recovered and removed by continuous washing with hydrated ethanolic solvent. Finally, the amidation products (FDWCNT) were dispersed in water and utilize for membrane fabrication.

2.3. Fabrication of membrane

For fabricating the membranes, each colloidal dispersion of 0.2 %

FDWCNT was vacuum filtrated through Polysulfone (PSf) support membrane under intense vapor pressure. During the vacuum suction, the CNT dispersions were uniformly distributed over the membrane support, where the vacuum pump exerted continuous suction force towards a rapid movement of water and overcame the electrostatic repulsion among the individual CNT layers and hence an ordered laminated CNT layer over PSf support is obtained which can be observed from the FESEM images. The membrane containing L-tryptophan and L-DOPA functionalized DWCNT as chiral selectors were named $M_{L\text{-}tryp}$ and $M_{L\text{-}DOPA,}$ respectively.

2.4. Characterization of FDWCNT based membranes

Chemical modification of the DWCNT into FDWCNT was analyzed via FT-IR analysis (Perkin Elmer, 2000 spectrophotometer). The surface morphology of the FDWCNT nanocomposite membrane was evaluated by AFM (WITec Atomic Force Microscope alpha 300 A). The membrane samples were analyzed by FESEM applying an electrical potential of 3 kV (FESEM, LEO 1427 VP, UK) and High-Resolution Transmission Electron microscopy (HRTEM, JEOL, Japan, JEM 2100). The elemental composition and the corresponding binding energy value of the involved hybrid orbitals in the FDWCNT and the prepared membranes were characterized by X-ray-assisted photoelectron spectroscopic technique (XPS) equipped with monochromatic radiation of Al Kα at a potential of 1486.6 eV. The electrical potential developed across the polymeric membrane surface was characterized by SurPASS™ Electrokinetic Analyzer. The measurement of streaming potential was done using standard Helmholtz-Smoluchowski Equations in terms of eV. The hydrophilic and hydrophobic nature of nanocomposite polymeric membrane was examined using standard contact angle analyzer having solvent media of water, (DM-501, Kyonea Interface Science) under room temperature. The dynamic mechanical stimulation of the membranes was recorded using Universal Tensile Testing Machine (AEC 1112-5 KN ACD).

2.5. Pressure-driven testing of the membrane via chiral separation experiments

Before performing the permeation experiments, the racemic mixture of DOPA and D-DOPA is standardized through an effective separation process of UHPLC analysis. The retention time corresponding to the relative peak area observed for D-DOPA and L-DOPA are 7.103 and 6.513, respectively. The results obtained from the complete 8 h of membrane permeation experiment are compared with the standard spectra of individual isomers. This quantitative estimation has given a better permeability rate of D-DOPA across the membrane surface and effective cross-linking of L-isomer within the hybrid membrane matrix. The related permselective properties, the physicochemical behavior of FDWCNT nanocomposite membranes were examined based upon our previously reported data [14].

The membrane performance was carried out through the permeation of racemic DOPA, which was independently measured using a series setup of three membrane cells containing three FDWCNT membranes of surface area 20 cm^2 each. The schematic diagram of the experimental design is given in Fig. 1. The feed side of the membrane was fitted with a dimensionless ring-shaped holder, which can provide a separation barrier seal towards feed and permeate chambers to distinguish the permeability of feed solution. The feed was circulated through the membrane applying pressure in a continuous process during the whole experiment. While the upper compartment of the membrane cell was filled with the aqueous enantiomeric solution, the enantiomers interacted with the reactive recognition sites on the membrane due to the self-association of isomers. The aqueous permeate side created the concentration gradient over the thin layered membrane barrier. The sample was collected from the permeate side at a regular time interval of 1 h and analyzed by UHPLC using the UHPLC model Dionex (Thermo Fisher Co.).

In UHPLC analysis, the three time-independent tests of the same sample result in the average value, with a standard error of ±2%. The analysis was done with a chiral column, CHIROBIOTIC ® T (column diameter 25 cm × 4.6 mm, 5 μm). Their absorption maxima were detected at a wavelength of 205 nm. The mobile phase used was 0.02%

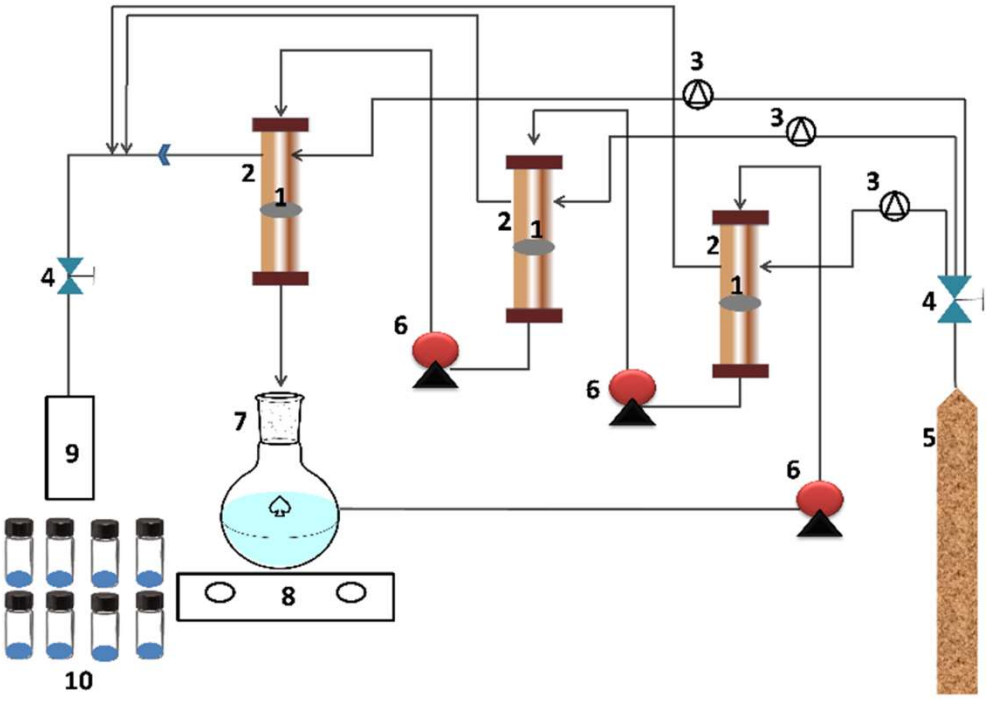

Fig. 1. Schematic diagram of the experimental setup (1) $M_{L\text{-}tryp}/M_{L\text{-}DOPA}$ membrane, (2) Two-compartment cell, (3) Pressure gauze, (4) Valve, (5) N_2 cylinder, (6) Peristaltic pump, (7) Feed solution reservoir, (8) Magnetic stirrer, (9) Gas outlet and (10) Sample viles.

of the equimolar mixture of aq. HCOOH and methanol at a flow rate of 0.5 mL min^{-1}. The resulting chromatogram of UHPLC analysis leads to the considerable peak area compared with calibration curves to resolute the concentration of a particular enantiomer in a quantified manner.

The flux, J ($mmolm^{-2}h^{-1}$) was calculated using Eq. (1)

$$J = \frac{V\Delta C}{A\Delta t} \tag{1}$$

where V is the feed or permeate phase volume, ΔC the concentration variation in the corresponding aqueous solutions at the time increment, Δt and A are the membrane area. A standard Eq. (2) of enantiomeric excess (%ee) was used to estimate D-DOPA present in the permeate solution versus L-DOPA quantitatively.

$$\%ee = \frac{C_{D-DOPA} - C_{L-DOPA}}{C_{D-DOPA} + C_{L-DOPA}} \times 100 \tag{2}$$

where $C_{D\text{-}DOPA}$ and $C_{L\text{-}DOPA}$ correspond to the D- and L-isomer concentration at any time t, respectively [25].

3. Results and discussion

3.1. Characterization of FDWCNT

Pristine DWCNT and FDWCNT were characterized by different instrumental techniques such as Fourier Transform Infrared analysis, X-ray Photoelectron Spectroscopy and Field Emission Scanning Electron Microscopy. The preliminary characterization gave the spectral difference between both, which was initially determined by FTIR spectroscopy. KBr pellets were used to characterize the amine-functionalized DWCNT. Fig. 2 exhibits the FTIR spectra of pristine DWCNT and both FDWCNT. Few prominent peaks were observed in the case of FDWCNT while comparing the spectra of pure DWCNT. A peak in the range of 3400–3500 cm^{-1} is observed in the spectrum for both FDWCNTs because of the —OH stretching vibration. This weak and broad band is because of the existence of O—H functional groups on the DWCNT. This result from either moisture bound to the DWCNT or oxidation of pure DWCNT during the filtration step. The broad peak at 2750 cm^{-1} corresponds to the vibrational frequency of N—H bond in both the spectra, whereas both the spectra represent the C—H vibration at 2938 cm^{-1}. In Fig. 2(b) and (c), carbonyl stretching (C═O) appeared at stretching vibration of 1678 cm^{-1}. The existence of the NH_2 and C═O peaks validates the successful functionalization of pure DWCNT. In the case of FDWCNT$_{L\text{-}tryp}$, the additional bond present at 1335 cm^{-1} is due to the polar framework of carbon and nitrogen atom (C—N), which can exhibit extra stability to the CNT outer-layers through aromatic ring current.

Further, Pristine DWCNT and FDWCNT were characterized by XPS and FESEM analysis. From the XPS analysis, the ratio of C/O and C/N were calculated using fitting protocol from photoelectron spectroscopy. The C/O and C/N ratio was calculated by deconvulating the XPS spectra of C1s and O1s, the sum of the coverage area of different functional groups of carbon and oxygen atoms, respectively. The area of every single peak of C1s spectra is proportional to the number of carbon atoms present in the relative functional groups. Therefore, the contribution of different functional groups are used to determine the total area covered by C1s high-resolution scan. The results were elaborately discussed in the supplementary material (Figs. S1 and S2).

3.2. Characterization of FDWCNT based nanocomposite membranes

Fig. 3 depicts the comparative overview of FTIR stretching frequencies of the chemical bonds introduced in $M_{L\text{-}tryp}$ and $M_{L\text{-}DOPA}$ membrane and compared with a bare Polysulfone (PSf) membrane. The characteristic vibrational frequencies at 1249, 1167 and 2911 cm^{-1} in Fig. 3(a) are attributed to the primary polysulfone membrane's C—O—C, O═S═O and alkyl moiety. In the FTIR spectra of the hybrid membranes, as shown in Fig. 3(b) and (c), the broad peak at around 3446.50 cm^{-1} indicates the vibrational stretching of the hydroxyl group due to the water-absorbing nature of the hybrid membranes. The absorption band at 3445 cm^{-1}, 2882 cm^{-1} and 1751 cm^{-1} are attributed to the vibrational scissoring and wagging of aromatic —OH, —NH of amide linkage and aromatic C═C bond, respectively. Both spectra in Fig. 3(b) and (c) represent the vibrational stretching of C═O and C═C at around 1678 and 1780 cm^{-1}. On account of the substituted hydroxyl group at the aromatic ring, their values entirely deviate from similarity [14,26]. In the case of L-tryptophan (Fig. 3(b)), the additional band present at 1349 cm^{-1} is due to the polar framework of carbon and nitrogen atom (C—N), which can exhibit extra stability to the CNT outer layers through aromatic ring current.

The characteristics binding energy value of amine treated FDWCNT based polymeric matrices were determined by XPS spectroscopy. Fig. S3 in the supplementary material has depicted the survey scan spectra of both the pure Polysulfone (PSf) and FDWCNT embedded nanocomposite membrane, including elemental composition. The quantitative attribution of a nitrogen atom (N) at $M_{L\text{-}DOPA}$ and $M_{L\text{-}tryp}$ has brought out their differentiative platform against raw polymeric M_{PSf}. The spectrograph has presented the standard binding overlap of p orbital of respective sulphur atom at 169 eV in Fig. S3. The most prominent overlapping of

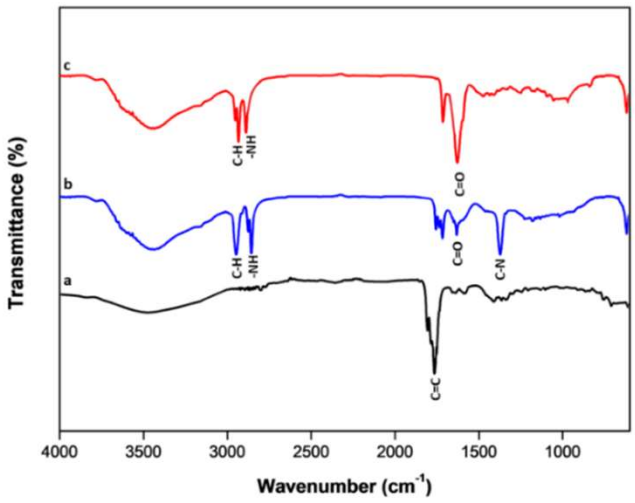

Fig. 2. FTIR spectra of (a) Pristine DWCNT (b) DWCNT functionalized using L-tryptophan, FDWCNT$_{L\text{-}tryp}$ (c) DWCNT functionalized using L-DOPA, FDWCNT$_{L\text{-}DOPA}$.

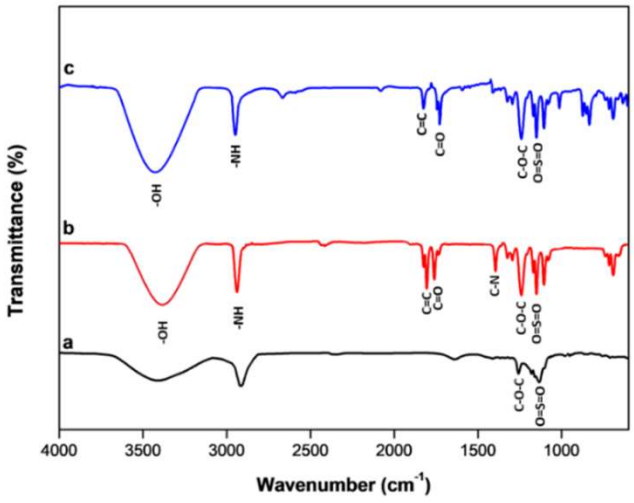

Fig. 3. FTIR spectra of (a) M_{PSf} (b) $M_{L\text{-}tryp}$ and (c) $M_{L\text{-}DOPA}$.

inner s-orbitals of carbon and oxygen atom are distinctly observed within the range of 286 eV and 534 eV, respectively. The high-resolution spectral scan of amino acid aggregated FDWCNT based hybrid membrane has given an additional depiction of binding energy value at 399.6 eV, mainly corresponding to the s-orbital overlap of guest N after functionalization in Fig. S3. The increase in the proportional ratio of O/C is critical for the quantitative estimation of oxygen at the functionalized polymeric membrane.

The integration of the broader peak of the C atom evaluated the presence of different covalent interactions, including C═O, C—S, C—N and C—H/C—C in the case of $M_{L\text{-}tryp}$ and $M_{L\text{-}DOPA}$, Fig. 4. The oxygen atom interacts with the carbon atom through two types of bonding (C—OH and C═O), with binding energy shifts at 286 and 286.5 eV. The comparatively lower electronegative nature of nitrogen and sulphur atom has shifted their binding interaction to 284.5 and 284 eV, respectively. The least polar alkyl and C—H have predicted their binding energy shift at 285 eV in both cases. The O1s high-resolution scan has depicted three peaks covering binding shift from 531 to 534 eV. The carbonyl bonding at a value of 531.5 eV has considerably brought out the broader attraction towards the functionalization route. The sp^2 hybridized orbital overlapping of sulphur and oxygen atom was visible at 532 and 533.5 eV. An intense sharp peak of hydroxyl linking with oxygen atom was obtained at a binding value of 534 eV. The binding energy shift of oxygen atoms in both L-tryptophan and L-DOPA-assisted polymeric matrices is comparatively similar due to their structural similarity of polysulfone. But it can be conferred that the notable difference is observed in the binding frequency of the nitrogen atom. Fig. 4 (A.4 and B.4) have presented the binding energy of nitrogen in terms of electron volt corresponding to the range of 399–400 eV. The differentiation of broader-shaped peaks in the case of the sulphur atom has evaluated the presence of C—S and O═S═O bond at a position of 167 and 169 eV, respectively [26].

The thermogravimetric estimation of the polymeric nanocomposite membrane was examined under a nitrogen atmosphere with a heat flow rate of 10 °C min^{-1} as shown in Fig. 5. For the M_{Psf} membrane, slight water weight loss was observed (at about 4.5 wt%), covering the temperature region of 60–120 °C. At the same time, $M_{L\text{-}tryp}$ and $M_{L\text{-}DOPA}$ undergo step-wise thermal decomposition relatively at higher temperatures due to the presence of amide linkage in the hybrid matrix. In addition to amide linkage, intermolecular hydrogen bonding is present among the substituted hydroxyl group of the L-DOPA in $M_{L\text{-}DOPA}$ membrane matrix [14,25]. Hence, the membrane containing L-DOPA

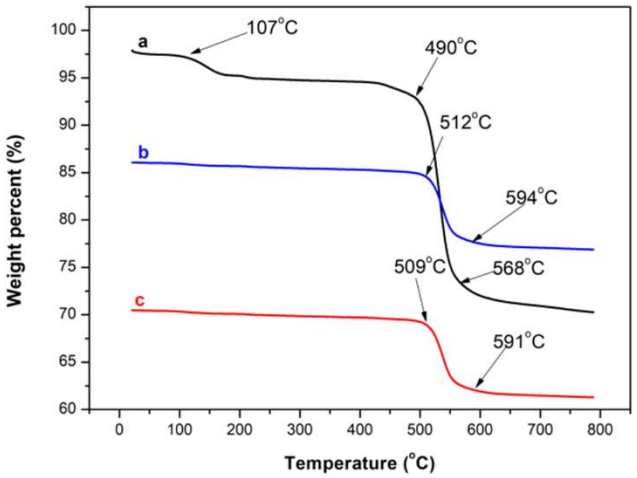

Fig. 5. TGA spectra of (a) M_{PSf} (b) $M_{L\text{-}tryp}$ (c) $M_{L\text{-}DOPA}$ membranes.

showed higher thermal stability up to 591 °C at the second step of mass loss than L-tryptophan.

The morphological analysis of the fabricated membranes was performed with FESEM analysis. The cross-sectional view of the composite membranes is shown in Fig. 6(A.1–A.2), which represents a lamellar structure consisting stacked of CNT laminates in an ordered manner, whereas Fig. 6(B.1–B.2) represents the frontier view on membrane surface representing a homogeneous distribution of FDWCNT over the spherical membrane pores. The raw PSf support cannot retain the water molecules within their microporous surface; also, it is not beneficial to possess chemical interactions towards organic moiety. Therefore, the membrane was modified by incorporating functionalized DWCNT impregnated with a chiral probe of L-DOPA and L-tryptophan through vacuum filtration techniques. In the cross-sectional image of prepared TFN membranes, it was observed that a thin amide layer was formed over a polymeric substrate which indicates that the amidation reaction successfully occurred at the edge of DWCNT. The cross-sectional morphology of membranes has shown the finger-like structure of PSf support in contact with the amide layer on the top surface. In the case of $M_{L\text{-}tryp}$, the nanoporous cavities are more efficient enough as compared to $M_{L\text{-}DOPA}$. This could be credited to the presence of an imidazolium ring adjacent to the benzene framework in the case of tryptophan, which

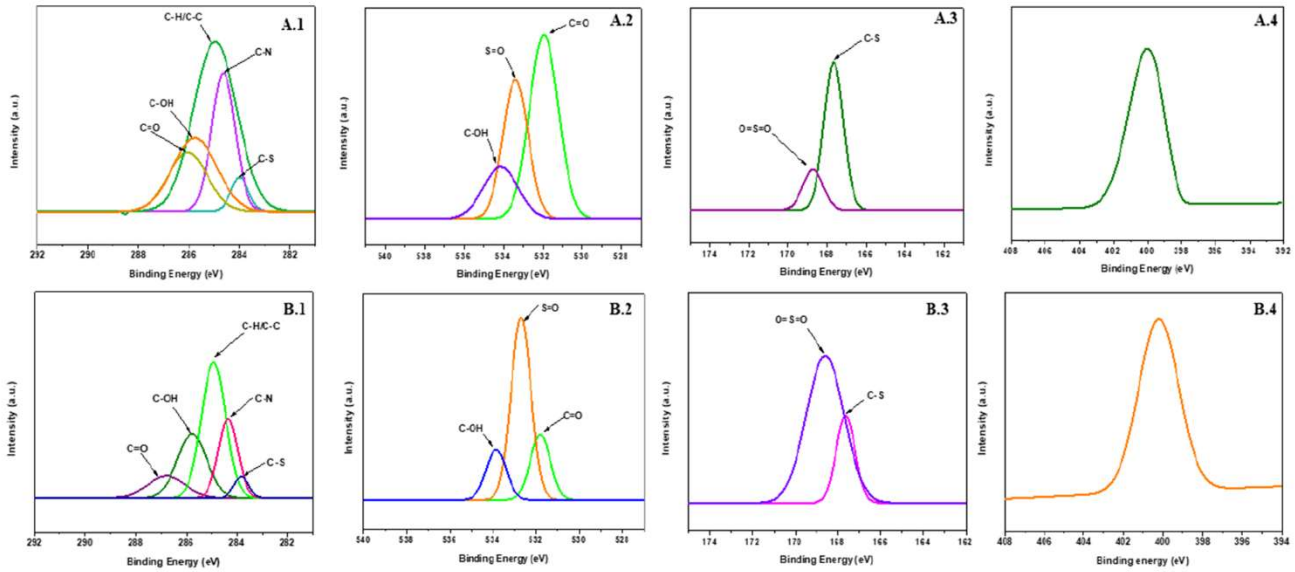

Fig. 4. XPS spectra of (A) $M_{L\text{-}tryp}$ (B) $M_{L\text{-}DOPA}$ membranes (A.1, B.1) C1s; (A.2, B.2) O1s; (A.3, B.3) S2p; (A.4, B.4) N1s high-resolution scan.

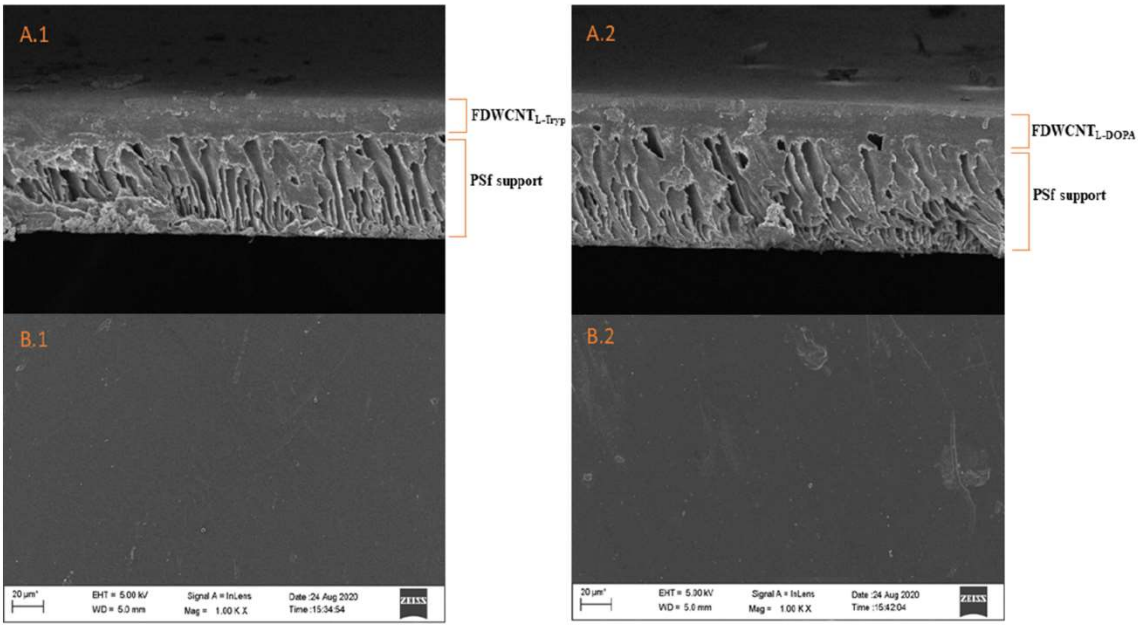

Fig. 6. FESEM images (A.1-A.2) Cross-sectional view; (B.1-B.2) Front view of $M_{L\text{-}tryp}$ and $M_{L\text{-}DOPA}$ membranes.

explored its aromatic stabilization and effective amide bond between C═O of COCl and NH_2 of tryptophan.

The Surface Probe Micrographs (AFM) of $M_{L\text{-}tryp}$ and $M_{L\text{-}DOPA}$ membranes given in Fig. 7 indicate a typical nodular (hills and valleys) morphology inherent to the surfaces. It was observed that the value of average roughness (R_a) of the $M_{L\text{-}tryp}$ and $M_{L\text{-}DOPA}$ membranes are 87 ± 0.4 and 33 ± 0.5 nm, respectively. Thus, it indicates that the inclusion of FDWCNT can unusually improve the roughness of the membrane. With the increment in the roughness of the membrane, the effective area for mass transfer increases, thereby increasing the mass transfer flux.

The determination of the hydrophilic or hydrophobic behavior of prepared $M_{L\text{-}tryp}$ and $M_{L\text{-}DOPA}$ is recognized as one of the chemical characteristics of the polymeric matrix. The variation of the surface energy of FDWCNT based polymeric matrix against liquid drop is evaluated by contact angle measurement using the standard sessile drop method. In Fig. 8, an angle formed by the liquid layer of the prepared membrane at the three-phase boundary surface is indicated with an arrowhead. The functionalization route dramatically enhances the

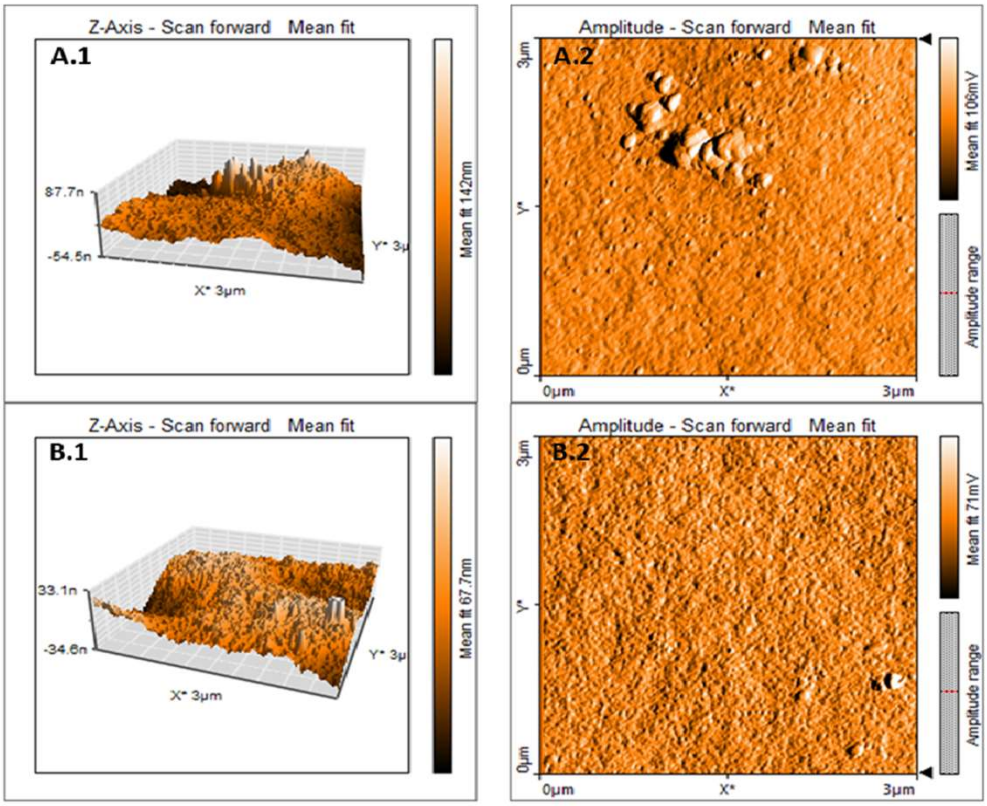

Fig. 7. AFM images (A.1, A.2) $M_{L\text{-}DOPA}$ (B.1, B.2) $M_{L\text{-}tryp}$ membranes.

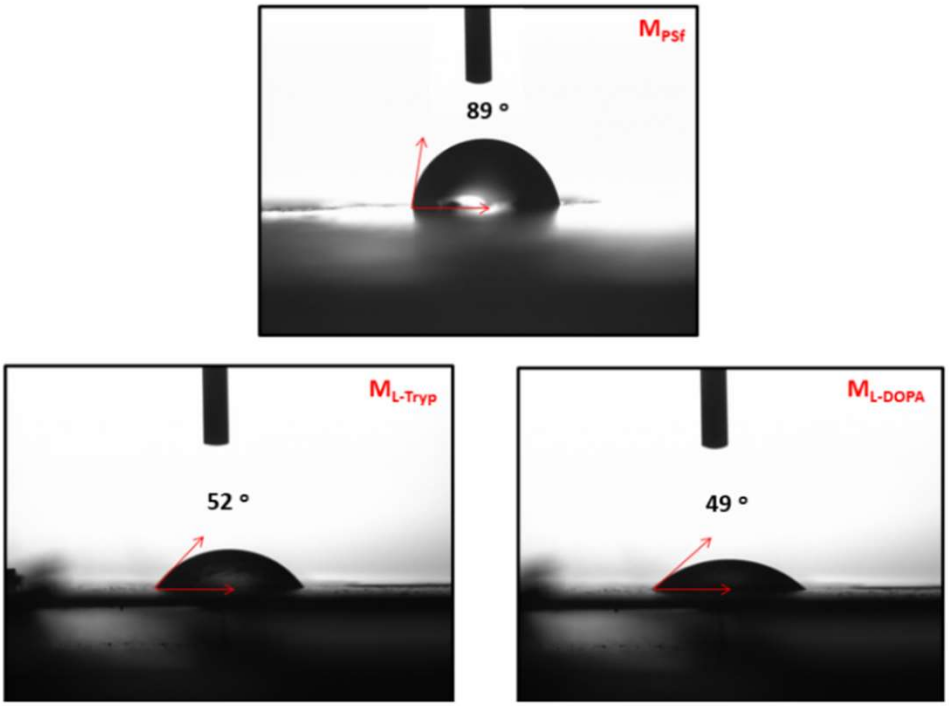

Fig. 8. Graphical representation of contact angle measurement of (a) M_{PSf}, (b) $M_{L\text{-}tryp}$ and (c) $M_{L\text{-}DOPA}$ membranes.

standard hydrophilicity of carbon nanotubes. Therefore, the concentration of L-DOPA and L-tryptophan on the DWCNT surface has offered a tremendous effect on the rate of increase of membrane hydrophilicity with an instant lowering of liquid density followed by increasing the pore size to a more considerable extent. It became a significant way to allow the quick passage of water molecules with isomeric resolution. The reactive amide surface of $M_{L\text{-}tryp}$ and $M_{L\text{-}DOPA}$ has controlled the optimum hydrophilicity compared to simple polysulfone membranes. Intermolecular hydrogen bonding between the water droplet and membrane surface is a driving force for membrane hydrophilicity [27]. The hydrophilic nature of the membrane could render the rate of aggregation of particles over the interface and therefore reduce the fouling behavior of the membrane [28]. The adequate hydrogen bonding of L-DOPA is due to hydroxyl moiety at the edge of the benzene ring, which can prevent the clogging of water molecules on the membrane surface.

The pH-dependent streaming potential method was used to determine electrokinetic measurement across M_{PSf}, $M_{L\text{-}tryp}$ and $M_{L\text{-}DOPA}$. In Fig. 9, the corresponding zeta potential values of the membrane were plotted as a function of pH. The $M_{L\text{-}DOPA}$ membrane containing L-DOPA with its negatively charged hydroxyl group at the edge surface contributes to a higher zeta potential value than the $M_{L\text{-}tryp}$. Therefore, the zeta potential value of $M_{L\text{-}DOPA}$ approaches −15 mV with increased pH via charge formation followed by adsorption. The negligible magnitude zeta potential value for the M_{PSf} can be attributed to the lack of functional groups on its surfaces [29].

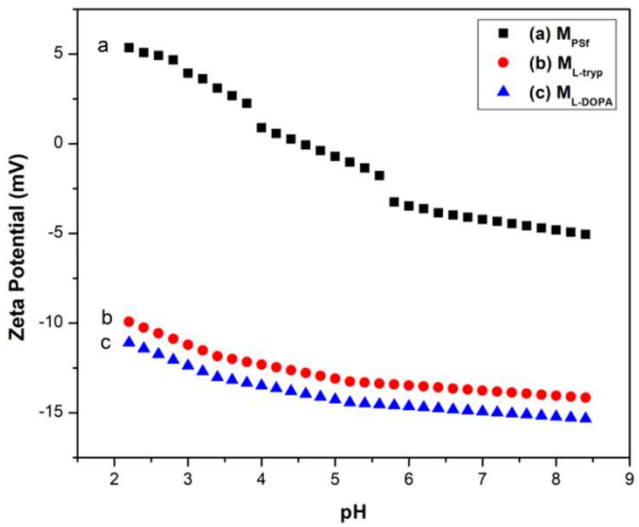

Fig. 9. Zeta Potential of (a) M_{PSf} (b) $M_{L\text{-}tryp}$ and (c) $M_{L\text{-}DOPA}$ membranes.

3.3. Racemic fractionation via pressure-driven permeation experiments

The enantiomeric racemic mixture of DOPA was resolved through a membrane permeation experiment as described in Section 2.5. The impact of one of the essential parameters like permeation time on the separation behavior of racemic mixture is shown in Fig. 10, which gives a clear depiction of the gradual decrease in flux rate with an increase in the permeation time and finally get saturated after 8 h. We observed a tradeoff between permeation and enantiomeric excess in both the membranes where the initial high permeation flux gradually declines until the saturation point with a concomitant gradual escalation of enantiomeric excess, as shown in the figure. The inconsistency in the permeation flux of the complementary isomer arose when L-isomer was preferentially adsorbed into the hybrid membrane matrix bearing the chiral probe via effective non-bonding interaction. Once chiral recognition with such specific binding is initiated, more and more of the same isomer tends to get adsorbed with noncovalent interaction through proper orientation of NH_2 [14,25]. Meanwhile, the D-isomer unable to find any friendly environment to get incorporated in the membrane matrix passes through it, resulting in a high enantiomeric excess performance. In $M_{L\text{-}DOPA}$ membrane, the hydrogen bonding exhibited by the hydroxyl group of L-DOPA can also contribute to such specific binding, which valid their higher enantioselective resolution (%ee = 99%) for the racemic mixture of DOPA, as compared to M_{tryp} membrane (%ee = 98 %) with no such hydrogen bonding.

The dependence of enantiomeric excess and permeation flux on racemates feed concentration is evaluated and illustrated in Fig. 11. The

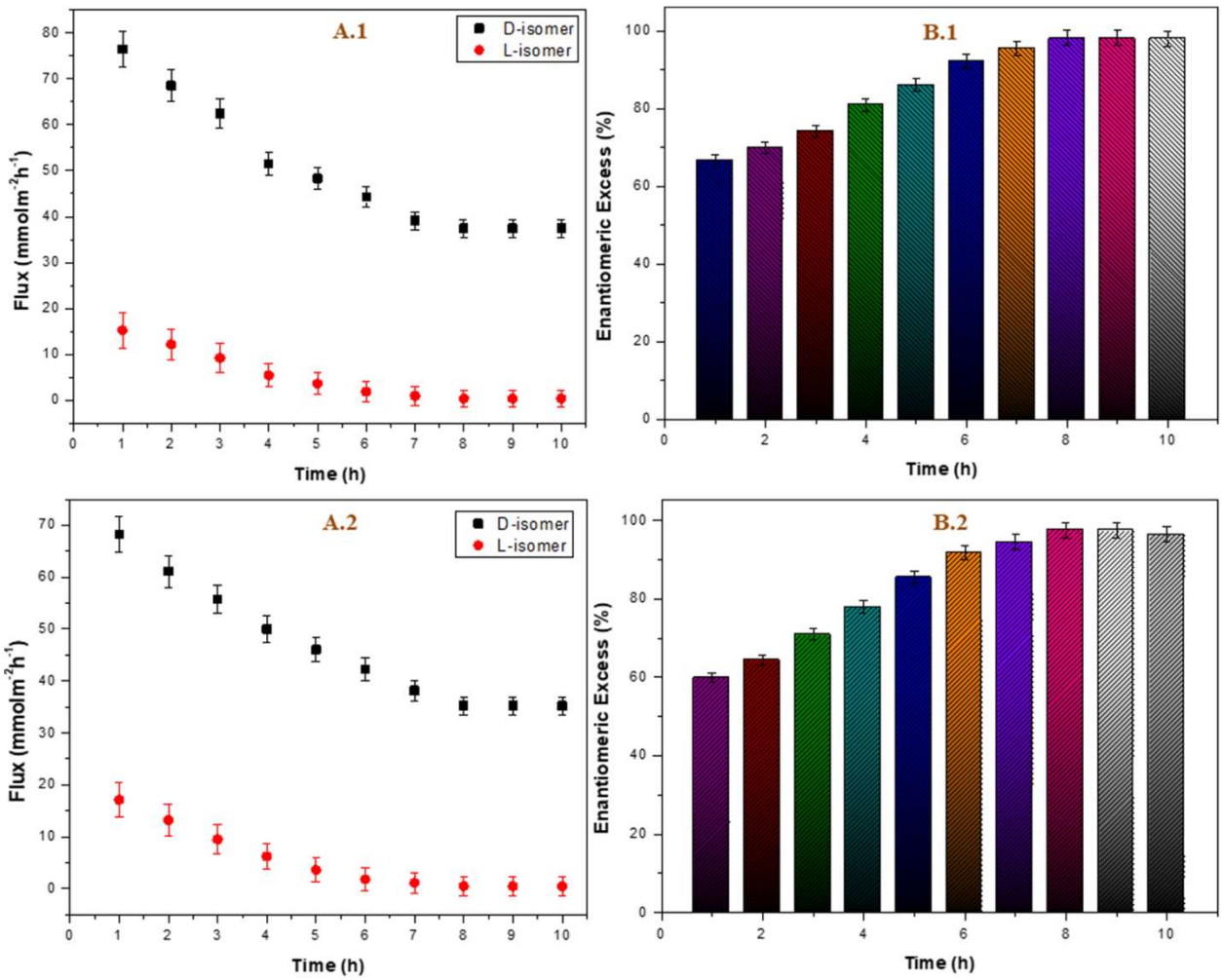

Fig. 10. Time-dependent variation of membrane flux and enantiomeric excess for $M_{L\text{-}DOPA}$ (A.1, B.1) and $M_{L\text{-}tryp}$ (A.2, B.2) respectively, where feed concentration: 1 mmol.L^{-1}, flow rate: 25 mL.min^{-1}, transmembrane pressure: 4 bar, temperature: 35 °C.

membrane flux gradually increases with an increase in racemates feed concentration and achieves a point of saturation at a concentration of 4 mmol.L^{-1}. Again, the lower flux values of L-isomer in the case of both membranes have demonstrated effective recognition with a chemical interaction. However, in both cases, the enantiomeric excess values followed a downtrend with the racemates feed concentration increase. The observed trend can be described in terms of concentration polarization within the hybrid membrane skeleton. Due to severe steric conditions, the rise in feed solution concentration has greatly perturbed the polarizability and polarizing power of individual charged species. This deduction of the polarity factor has suppressed the integration of chiral isomer [14,25]. Hence, an increase in feed concentration favors isomeric agglomeration over membrane surface instead of effective recognition with a chemical interaction. A substantial amount of L-isomer also gets passed through the membrane matrix, which eventually suppressed the resolution performance.

The influence of trans-membrane pressure on the enantioseparation performance of the fabricated membranes was also investigated and is shown in Fig. 12. With a gradual increment of transmembrane pressure, the apparent flux values decrease due to the development of intermolecular collision, which disrupts the diffusion flow within the membrane matrix. The turbulent flow of the racemic mixture becomes asymptotic at around 5 bar pressure and such pressure, L-isomer undergoes covalent bonding interaction over the reactive polymeric platform, which can be ascribed from the adsorptive grafting of L-isomer to functionalized DWCNT [14]. Further increment in the pressure value at 5 bar showed stability of L-isomer within the compressed molecular structure and hence the more excellent ee% value.

The separation mechanism of the racemic mixture of DOPA is primarily based on the stereo-specific interaction between the chiral recognition site and one of the individual enantiomers. Therefore, the three-point interaction is an essential critical model to quantify the interaction affinity of different groups attached to the chiral center of the isomer, where one enantiomer-chiral probe configuration could have three interaction (two hydrogen bonds and one π-π interaction) whereas the other corresponding configuration could only have two interactions due to steric hindrance. Furthermore, recent Molecular dynamics simulations suggest that for polymeric chiral stationary phases (CSP) with numerous possible interaction sites subjected to swelling, a dynamic interaction mode of chiral recognition mechanism is more reasonable than a static interaction mechanism based on static three-point model [31]. Within the scope of dynamic nature of the molecular recognition process, basically, it is assumed that solute makes a large number of encounters with the polymeric CSP, resulting in the rapid formation, breaking, re-formation of hydrogen bonds either in between donors on the solute to the acceptors on the polymer, or acceptors on the solute to the donors on the polymer [32]. Meanwhile, the repulsive interaction arising between bulky groups such as rings on drug substrate and polymer regulates the extent of attractive interaction between donor–acceptor via adjusting the available interacting space between them. Since both the enantiomers of the drug possess different spatial orientations with respect to the chiral polymer, the extent of repulsive

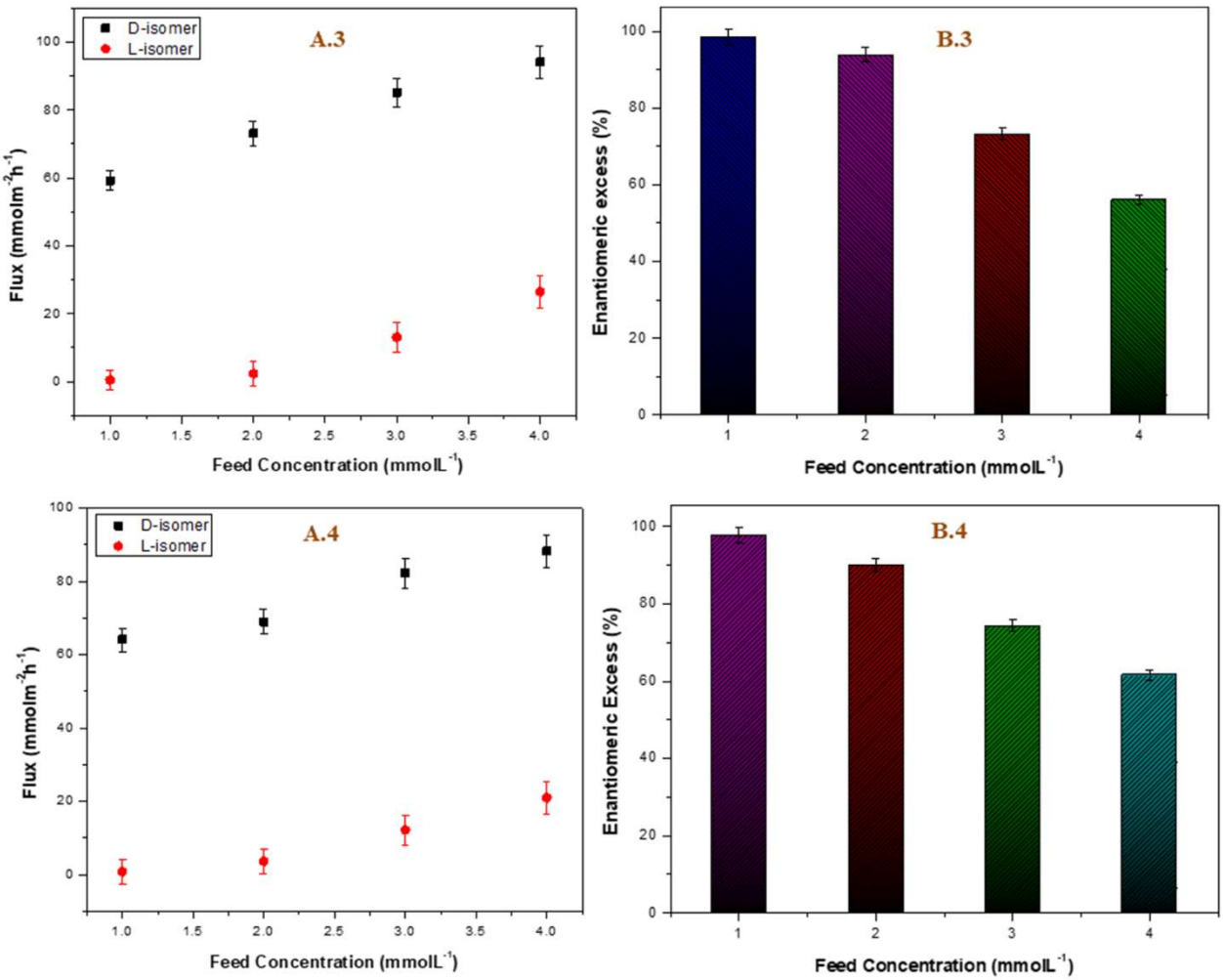

Fig. 11. Variation of membrane flux and enantiomeric excess for feed concentration for $M_{L\text{-}DOPA}$ (A.3, B.3) and $M_{L\text{-}tryp}$ (A.4, B.4) respectively, where flow rate: 25 mL.min^{-1}, trans-membrane pressure: 4 bar, temperature: 35 °C.

interaction will be distinctly different for both the isomers, leading to different hydrogen-bonding opportunities and eventually discriminated the two enantiomers. The chiral resolution efficiency under the dynamic recognition process is also dependent on the identity of the mobile phase solvent, as different solvents lead to varying extents of H-bonding interaction which is the key factor in governing the chiral resolutions [33]. This might be another factor contributing to the enantioselective performance of the chiral polymeric membranes. Since in the present study, the active chiral separating layer is a FDWCNT rather than a polymer where the polysulfone acts as a support to the active layer. Compared to polymer, DWCNT is more reluctant to swelling. Hence, the primary factor considered is the static three-point interaction model to interpret the observed chiral resolution mechanism.

The enantioselective adsorption behavior of $M_{L\text{-}DOPA}$ and $M_{L\text{-}tryp}$ exhibited a stronger binding affinity with the L-isomer of the racemic mixture of DOPA. In these respective membranes, the pressure gradient efficiently acted as a driving force. In addition to this, the higher enantiomeric excess of L-DOPA may be due to the non-bonding interaction of hydrogen groups shown by the four different groups attached to the chiral center with the L-isomer of the racemic mixture of DOPA. The three-point stereo-specific interaction of L-DOPA also establishes the proper orientation of functional groups. Whereas, in the case of L-tryptophan, the orientation of the groups is deviated from their specific position due to the combined effect of aromaticity and steric crowding of indole. Therefore, it exhibits the smaller value of % ee in the case of $M_{L\text{-}tryp}$. The schematic diagram illustrating the possible mechanism behind chiral separation is depicted in Fig. 13.

Furthermore, the ratio of bulk convective velocity to the diffusive velocity can be measured as Peclet number for both the membrane permeation experiments at ~500. This can be calculated by converting flux value to a velocity coefficient in multiplicative of membrane area (i.e., 0.002 ms^{-1}), with an inverse relationship to the diffusivity of L-DOPA and L-tryptophan [30]. The Peclet number is used in the sense that diffusion enhances the rate of convection. The more excellent value of the Peclet number yields greater fluid volume processed through recyclable manner within a considerable time. This membrane permeation is highly valued towards a point of commercialization compared to the conventional chromatographic process. The convective flow of fluid through packed column material generally suffers very much inert atmosphere. Hence, it exhibits a lower value of convective velocity, which is highly favored under composite membrane surfaces. The diagram below shows the elution of one of the isomers through a membrane-based stationary phase as predicted, where obtained chromatogram presented one of the isomers in high retention time over others, Fig. 14. Therefore, the performance of the chiral stationary phase is expected to be based on the chemically induced binding affinity of one of the isomers to the chiral packed stationary phase and then eluted fractionally. However, our prepared enantioselective chiral membranes have pointed out their industrial applications as chiral stationary phase in a chromatographic column. The use of low-cost, high selective TFN membranes as chiral stationary phase in a chromatographic column will provide a new strategy for the separation processes. It will be highly

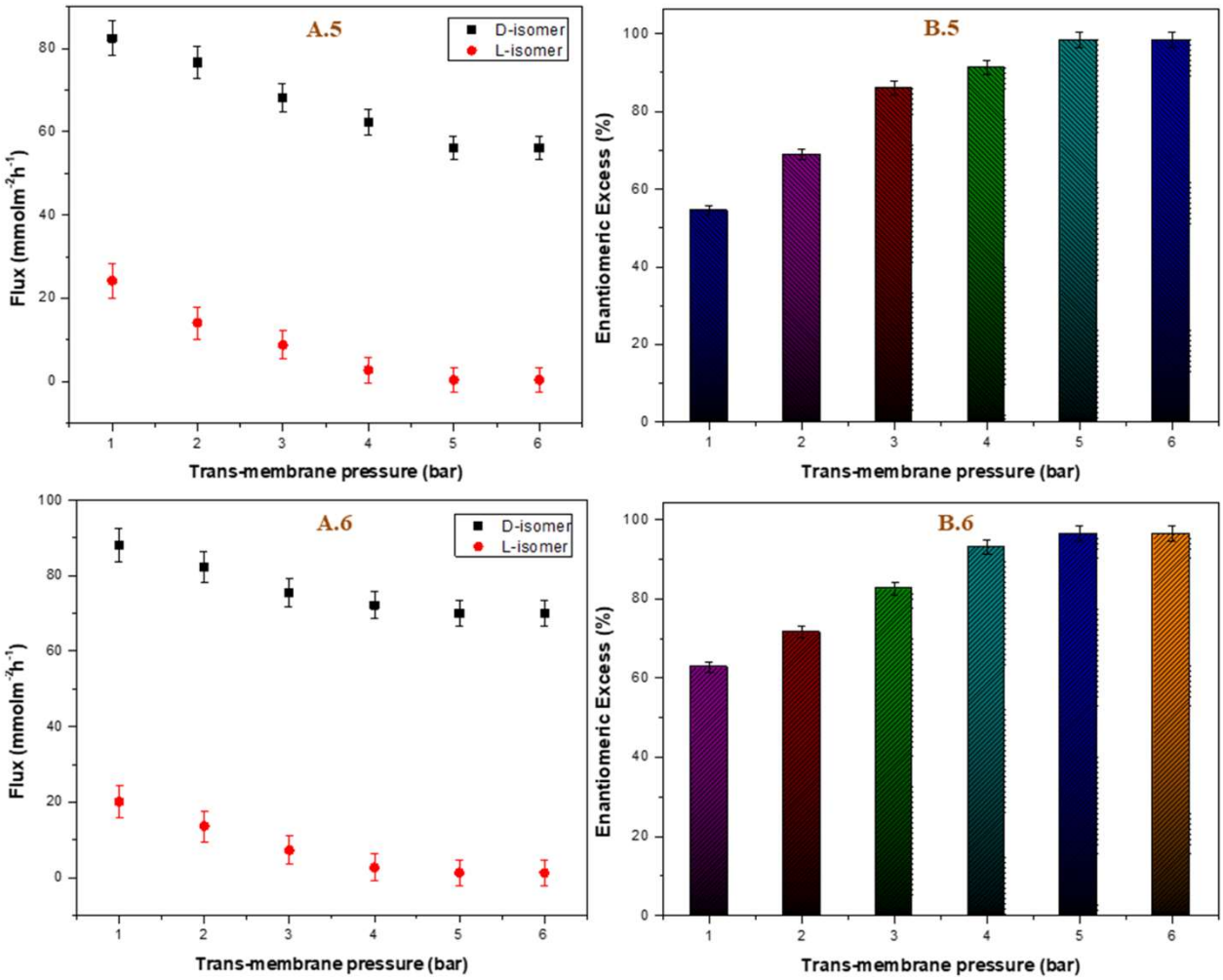

Fig. 12. Pressure-dependent variation of membrane flux and enantiomeric excess of $M_{L\text{-}DOPA}$ (A.5, B.5) and $M_{L\text{-}tryp}$ (A.6, B.6) respectively, where feed concentration: 1 mmol.L^{-1}, flow rate: 25 mL.min^{-1}, temperature: 35 °C.

promising for the bulk selective resolution of the enantiomeric mixture.

3.4. The reproducibility of the $M_{L\text{-}DOPA}$ and $M_{L\text{-}tryp}$ membranes

The reproducibility of a membrane is considered a crucial factor affecting the rate of industrial mass production. Therefore, despite having excellent chiral separation performance, the membrane $M_{L\text{-}DOPA}$ and $M_{L\text{-}tryp}$ have also tested for their reproducibility. To investigate the reproducibility of the two nanocomposite membranes, three batches of each $M_{L\text{-}DOPA}$ and $M_{L\text{-}tryp}$ membranes were prepared based on the conditions previously mentioned in Section 2.3 and performed the permeation experiment for membrane performance study. The permeation experiments were conducted using the same membrane cell applying the same conditions, like feed concentration of racemic DOPA is 1 mmol.L^{-1}, flow rate of 25 mL.min^{-1}, transmembrane pressure of 4 bar, and a constant temperature of 35 °C. The results of each $M_{L\text{-}DOPA}$ and $M_{L\text{-}tryp}$ membrane are shown in Table 1. Interestingly, all six membranes exhibited almost the same separation selectivity, with the earlier membranes yielding nearly high % ee values. The results suggested that the chiral separation properties of both membranes remained the same in every batch, which confirms both membranes' reproducibility.

3.5. Theoretical interaction study of the isomers with $FDWCNT_{L\text{-}DOPA}$ and $FDWCNT_{L\text{-}tryp}$

To establish the three-point interaction between L-DOPA with $FDWCNT_{L\text{-}DOPA}$ and $FDWCNT_{L\text{-}tryp}$, we have calculated the interaction energy from optimized energy values obtained from semi-empirical (Austin Model-1, AM1) calculations in Gaussian 09 software. First of all, we have optimized $FDWCNT_{L\text{-}DOPA}$, $FDWCNT_{L\text{-}DOPA}$, L-DOPA and D-DOPA individually. In the next step, optimized structures of L-DOPA and D-DOPA have been placed separately in the vicinity of $FDWCNT_{L\text{-}DOPA}$ and $FDWCNT_{L\text{-}tryp}$, respectively at different positions where the possibility of hydrogen bonding is high. The D- and L-counterparts of DOPA with $FDWCNT_{L\text{-}DOPA}$ and $FDWCNT_{L\text{-}tryp}$ of the chiral membrane were then subjected to semi-empirical AM1 calculations separately for interaction study between them and the predicted structures are shown in Fig. S7. The interaction energy was calculated using Eq. (3) given below:

$$\Delta E_{AB} = E_{AB} - (E_A + E_B) \tag{3}$$

where ΔE_{AB} is the interaction energy between $FDWCNT_{L\text{-}DOPA}$ with L-DOPA/D-DOPA and $FDWCNT_{L\text{-}tryp}$ with L-DOPA/D-DOPA, E_A is the energy of the $FDWCNT_{L\text{-}DOPA}$/$FDWCNT_{L\text{-}tryp}$ and E_B is the energy of the L-DOPA/D-DOPA.

The results of theoretical calculation were in compliance with the experimental results. The enantioselective adsorption behavior of $FDWCNT_{L\text{-}DOPA}$ and $FDWCNT_{L\text{-}tryp}$ exhibited the stronger binding affinity with the L-isomer of the racemic mixture of DOPA than the D-isomer. The adsorption of L-isomer onto the chiral membrane mainly involves hydrogen bonding interaction. From the results, it is seen that

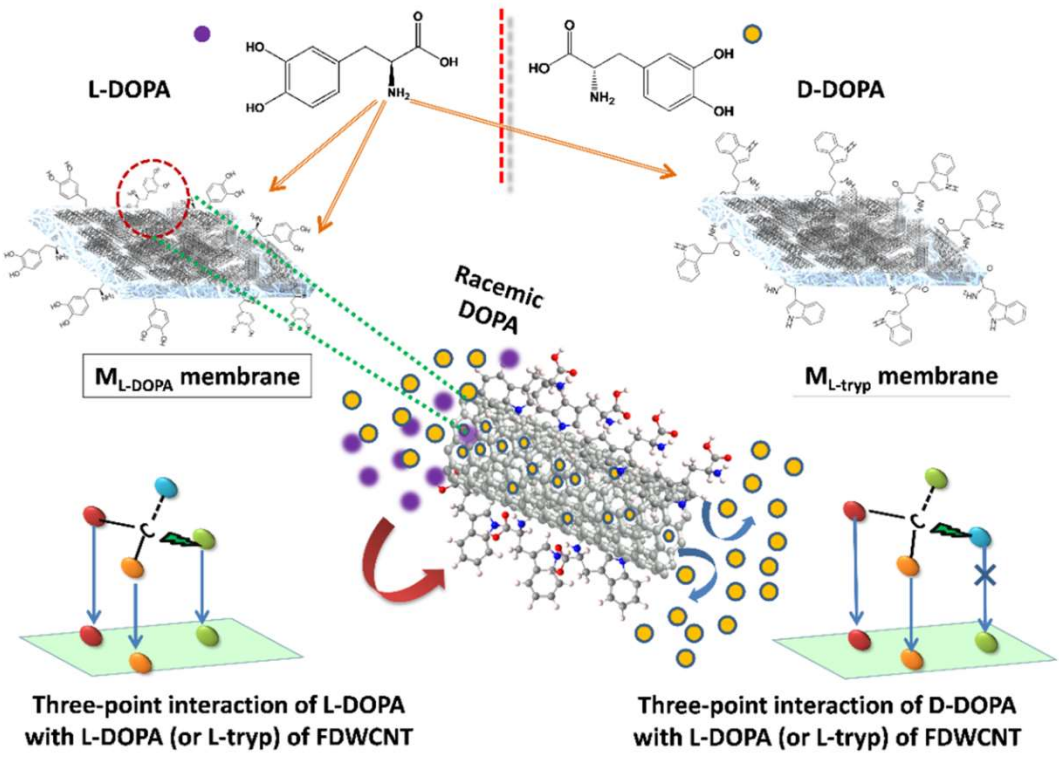

Fig. 13. Schematic representation of the possible mechanism behind chiral separation.

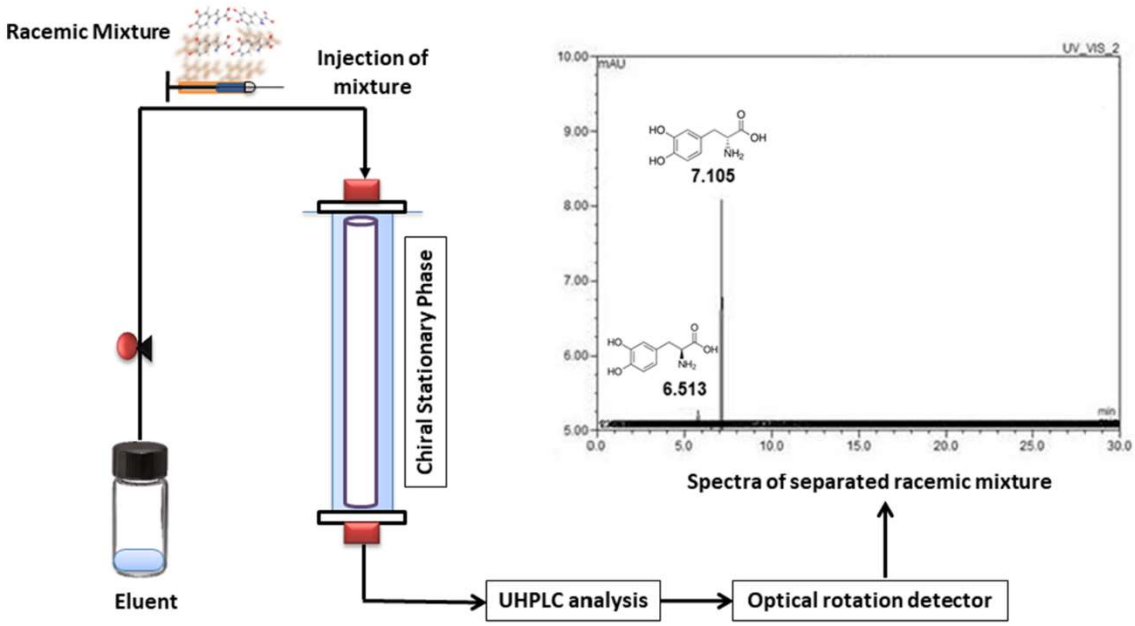

Fig. 14. Elution diagram depicting the performance of the chiral stationary phase.

the interaction energy between L-DOPA and $FDWCNT_{L\text{-}DOPA}$ was found to be –32.72 $kJ.mol^{-1}$, D-DOPA and $FDWCNT_{L\text{-}DOPA}$ was −28.76 $kJ.mol^{-1}$, L-DOPA and $FDWCNT_{L\text{-}tryp}$ was −25.71 $kJ.mol^{-1}$, and D-DOPA and $FDWCNT_{L\text{-}tryp}$ was – 24.88 $kJ.mol^{-1}$ respectively. This observation implies a better binding of the L-isomer of DOPA with the $FDWCNT_{L\text{-}DOPA}$ and $FDWCNT_{L\text{-}tryp}$.

4. Conclusion

The current work has summarized that the amino acid residues in L-tryptophan and L-DOPA act as a progressive source of functionalization probe incorporated within bi-layered graphene sheets in a rolling manner. The change in the rheological properties due to structural deformation of DWCNT upon step-wise covalent functionalization was analyzed by conventional spectroscopic and electron diffraction methods. Eventually, two different nanocomposite membranes ($M_{L\text{-}tryp}$ and $M_{L\text{-}DOPA}$) were developed via vacuum-assisted filtration technique by introducing the amide functionalized DWCNT into the membrane matrix and characterized using various spectroscopic methods. The effectiveness of each membrane towards the chiral separation of the

Table 1
Results of the Batch-wise chiral separation performance of $M_{L\text{-}DOPA}$ and $M_{L\text{-}tryp}$ membranes.

Membrane	Batch	%ee of D-DOPA over L-DOPA
$M_{L\text{-}DOPA}$	First	99.3 ± 0.2
	Second	99.18 ± 0.3
	Third	98.9 ± 0.4
$M_{L\text{-}tryp}$	First	98.85 ± 0.4
	Second	98.2 ± 0.4
	Third	97.98 ± 0.3

racemic mixture of DOPA was examined in terms of permeation experiments by optimizing permeation time, feed concentration and transmembrane pressure at a constant flow rate and temperature of 25 mL. min^{-1} and 35 °C, respectively. Due to the three-point interaction between the $FDWCNT_{L\text{-}DOPA}$/$FDWCNT_{L\text{-}tryp}$ and the L-isomer of the racemic mixture of DOPA, the L-isomer was preferentially adsorbed onto the membrane. This has been verified by the theoretical calculations of interaction energies between the specific components. In contrast, the D-isomer was permeated through the nanoporous membranes. The enantiomeric excess values were found to be 99% for the membrane containing L-DOPA as the chiral probe ($M_{L\text{-}DOPA}$) and 98% for the membrane containing L-tryptophan as the chiral probe ($M_{L\text{-}tryp}$), respectively. The concentration gradient developed across the charged membrane surface provided a substantial diffusion of both isomers on the excess of feed concentration. Therefore, the enantiomeric excess values go down to 20–40%. The peclet number for both the membranes was found to be ~500, which can be attributed to the higher convective velocity of the fluid through bulk transport phenomena in a continuous manner. Based on the above results, the highly reproducible FDWCNT based polymeric nanocomposite membrane approach become a suitable and energy-efficient pathway towards the chiral separation of organic drugs.

CRediT authorship contribution statement

Monti Gogoi: Methodology, Software, Formal analysis, Investigation, Resources, Data curation, Writing – original draft, Writing – review & editing. **Rajiv Goswami:** Software, Writing – original draft. **Alimpia Borah:** Formal analysis, Investigation, Resources, Data curation, Writing – original draft. **Hrishikesh Sarmah:** Methodology. **Parashmoni Rajguru:** Software. **Swapnali Hazarika:** Conceptualization, Visualization, Methodology, Validation, Writing – review & editing, Supervision, Project administration, Funding acquisition.

Declaration of Competing Interest

The authors declare that they have no known competing financial interests or personal relationships that could have appeared to influence the work reported in this paper.

Acknowledgment

The authors are grateful to Dr G Narahari Sastry, Director, CSIR-NEIST, for his keen interest in the subject and for approving the manuscript for publication with Reference No. NMN-202140.

Appendix A. Supplementary material

Supplementary data to this article can be found online at https://doi.org/10.1016/j.seppur.2021.119704.

References

[1] B. Schuur, B.J.V. Verkuijl, A.J. Minnaard, J.G. de Vries, H.J. Heeres, B.L. Feringa, Chiral separation by enantioselective liquid-liquid extraction, Org. Biomol. Chem. 9 (1) (2011) 36–51.
[2] E. Sanganyado, Z. Lu, Q. Fu, D. Schlenk, J. Gan, Chiral pharmaceuticals: A review on their environmental occurrence and fate processes, Water Res. 124 (2017) 527–542.
[3] L. Zhao, L. Yang, Q. Wang, Silica-based polypeptide-monolithic stationary phase for hydrophilic chromatography and chiral separation, J. Chromatogr. A 1446 (2016) 125–133.
[4] S.Y. Lau, F.N. Gonawan, S. Bhatia, A.H. Kamaruddin, M.H. Uzir, Conceptual design and simulation of a plant for the production of high purity (S)-ibuprofen acid using innovative enzymatic membrane technology, Chem. Eng. J. 166 (2) (2011) 726–737.
[5] H. Tan, T. Liu, X. Zhang, Q. Shan, J. Chen, Z. Li, H. Ihara, H. Qiu, Preparation of Vortex Porous Graphene Chiral Membrane for Enantioselective Separation, Anal. Chem. 92 (20) (2020) 13630–13633.
[6] F. Ahmadi, E. Yawari, M. Nikbakht, Computational design of an enantioselective molecular imprinted polymer for the solid phase extraction of S-warfarin from plasma, J. Chromatogr. A 1338 (2014) 9–16.
[7] H. Tan, X. Zhang, Z. Li, H. Qiu, Small-Scale Nanoparticles Pyrolyzed from Layered Hydrotalcite between Graphene Interlayers as Intermediates for Self-Assembly into Metal Oxide Nanosheets and Hollow Nanospheres, ChemNanoMat 6 (8) (2020) 1270–1275.
[8] R. Xie, L.-Y. Chu, J.-G. Deng, Membranes and membrane processes for chiral resolution, Chem. Soc. Rev. 37 (6) (2008) 1243, https://doi.org/10.1039/b713350b.
[9] H. Han, W. Liu, Y. Xiao, X. Ma, Y. Wang, Advances of enantioselective solid membranes, New J. Chem. 45 (15) (2021) 6586–6599.
[10] X. Hou, T. Xu, Y. Wang, S. Liu, R. Chu, J. Zhang, B.o. Liu, Bo Liu, Conductive and Chiral Polymer-Modified Metal-Organic Framework for Enantioselective Adsorption and Sensing, ACS Appl. Mater. Interfaces 10 (31) (2018) 26365–26371.
[11] C. Meng, Q. Chen, X. Li, H. Liu, Controlling covalent functionalization of graphene oxide membranes to improve enantioseparation performances, J. Membr. Sci. 582 (2019) 83–90.
[12] C. Yin, W. Chen, J. Zhang, M. Zhang, J. Zhang, A facile and efficient method to fabricate high-resolution immobilized cellulose-based chiral stationary phases via thiol-ene click chemistry, Sep. Purif. Technol. 210 (2019) 175–181.
[13] S. Paladhi, I.S. Hwang, E.J. Yoo, D.H. Ryu, C.E. Song, Kinetic Resolution of β-Hydroxy Carbonyl Compounds via Enantioselective Dehydration Using a Cation-Binding Catalyst: Facile Access to Enantiopure Chiral Aldols, Org. Lett. 20 (2018) 2003–2006.
[14] M. Gogoi, R. Goswami, P.G. Ingole, S. Hazarika, Selective permeation of L-tyrosine through functionalized single-walled carbon nanotube thin film nanocomposite membrane, Sep. Pur. Tech. 233 (2020), 116061.
[15] C. Meng, Y. Sheng, Q. Chen, H. Tan, H. Liu, Exceptional chiral separation of amino acid modified graphene oxide membranes with high-flux, J. Membr. Sci. 526 (2017) 25–31.
[16] Y. Wang, R. Zhang, Z. Zhang, J. Cao, T. Ma, Host-Guest Recognition on 2D Graphitic Carbon Nitride for Nanosensing, Adv. Mater. Interfaces 6 (2019) 1901429.
[17] T.J. Konch, R.K. Gogoi, A. Gogoi, K. Saha, J. Deka, K.A. Reddy, K. Raidongia, Nanofluidic transport through humic acid modified graphene oxide nanochannels, Mater. Chem. Front. 2 (9) (2018) 1647–1654.
[18] M.H.O. Rashid, S.F. Ralph, Carbon Nanotube Membranes: Synthesis Properties, and Future Filtration Applications, Nanomaterials 7 (2017) 99.
[19] H.A. Shawky, S.-R. Chae, S. Lin, M.R. Wiesner, Synthesis and characterization of a carbon nanotube/polymer nanocomposite membrane for water treatment, Desalination 272 (1-3) (2011) 46–50.
[20] F.H. Gojny, M.H.G. Wichmann, U. Köpke, B. Fiedler, K. Schulte, Carbon nanotube-reinforced epoxy-composites: enhanced stiffness and fracture toughness at low nanotube content, Compos. Sci. Technol. 64 (2004) 2363–2371.
[21] D. Qian, G.J. Wagner, W.K. Liu, M.F. Yu, R.S. Ruoff, Mechanics of carbon nanotubes, Appl. Mech. Rev. 55 (2002) 495–533.
[22] T. Lin, V. Bajpai, T. Ji, L. Dai, Chemistry of carbon nanotubes, Aust. J. Chem. 56 (7) (2003) 635, https://doi.org/10.1071/CH02254.
[23] P.-C. Ma, N.A. Siddiqui, G. Marom, J.-K. Kim, Dispersion and functionalization of carbon nanotubes for polymer-based nanocomposites: A review, Composites Part A 41 (10) (2010) 1345–1367.
[24] S. Daer, J. Kharraz, A. Giwa, S.W. Hasan, Recent applications of nanomaterials in water desalination: a critical review and future opportunities, Desalination 367 (2015) 37–48.
[25] S. Hazarika, Enantioselective permeation of racemic alcohol through polymeric membrane, J. Membr. Sci. 310 (1-2) (2008) 174–183.
[26] R. Goswami, M. Gogoi, A. Borah, H. Sarmah, P.G. Ingole, S. Hazarika, Functionalized Activated carbon and carbon nanotube hybrid membrane with enhanced antifouling activity for removal of cationic dyes from aqueous solution, Environ. Nanotechnol. Monit. Manage. 16 (2021), 100492.
[27] M.R. Esfahani, J.L. Tyler, H.A. Stretz, M.J.M. Wells, Effects of a dual nanofiller, nano-TiO_2 and MWCNT, for polysulfone-based nanocomposite membranes for water purification, Desalination 372 (2015) 47–56.
[28] A.M. Ihsanullah, T. AlAmer, A. Laoui, N. Abbas, F. Al-Aqeeli, M. Patel, M. A. Khraisheh, N.H. Atieh, Fabrication and antifouling behavior of a carbon nanotube membrane, Mater. Des. 89 (2016) 549–558.

[29] N. Phao, E.N. Nxumalo, B.B. Mamba, S.D. Mhlanga, A nitrogen-doped carbon nanotube enhanced polyethersulfone membrane system for water treatment, Phys. Chem. Earth, Parts A/B/C 66 (2013) 148–156.
[30] J.J. Keating, S. Bhattacharya, G. Belfort, Separation of D, L-amino acids using ligand exchange membranes, J. Membr. Sci. 555 (2018) 30–37.
[31] X. Wang, C.J. Jameson, S. Murad, Modeling Enantiomeric Separations as an Interfacial Process Using Amylose Tris(3,5-dimethylphenyl carbamate) (ADMPC) Polymers Coated on Amorphous Silica, Langmuir 36 (2020) 1113–1124.
[32] X. Wang, D.W. House, P.A. Oroskar, A. Oroskar, A. Oroskar, C.J. Jameson, S. Murad, Molecular dynamics simulations of the chiral recognition mechanism for a polysaccharide chiral stationary phase in enantiomeric chromatographic separations, Mol. Phys. 117 (23-24) (2019) 3569–3588.
[33] B. Zhao, P.A. Oroskar, X. Wang, D. House, A. Oroskar, A. Oroskar, C. Jameson, S. Murad, The Composition of the Mobile Phase Affects the Dynamic Chiral Recognition of Drug Molecules by the Chiral Stationary Phase, Langmuir 33 (2017) 11246–11256.